Strong-disorder renormalization group study of $S=\frac{1}{2}$ Heisenberg antiferromagnet layers and bilayers with bond randomness, site dilution, and dimer dilution

Yu-Cheng Lin and Heiko Rieger

Theoretische Physik, Universität des Saarlandes, 66041 Saarbrücken, Germany

Nicolas Laflorencie

Department of Physics and Astronomy, University of British Columbia, Vancouver, British Columbia, Canada V6T 1Z1

Ferenc Iglói

Research Institute for Solid State Physics and Optics, H-1525 Budapest, Hungary
and Institute of Theoretical Physics, Szeged University, H-6720 Szeged, Hungary

Using a numerical implementation of a strong-disorder renormalization group, we study the low-energy, long-distance properties of layers and bilayers of $S=1/2$ Heisenberg antiferromagnets with different types of disorder: bond randomness, site dilution, and dimer dilution. Generally the systems exhibit an ordered and a disordered phase separated by a phase boundary on which the static critical exponents appear to be independent of bond randomness in the strong-disorder regime, while the dynamical exponent is a continuous function of the bond disorder strength. The low-energy fixed points of the off-critical phases are affected by the actual form of the disorder, and the disorder-induced dynamical exponent depends on the disorder strength. As the strength of the bond disorder is increased, there is a set of crossovers in the properties of the low-energy singularities. For weak disorder quantum fluctuations play the dominant role. For intermediate disorder non-localized disorder fluctuations are relevant, which become localized for even stronger bond disorder. We also present some quantum Monte Carlo simulation results to support the strong-disorder renormalization approach.

I. INTRODUCTION

The two-dimensional (2D) spin-1/2 Heisenberg antiferromagnet has attracted abiding interest in recent years, mainly motivated by its relation to high-temperature superconductivity.[1] According to the Mermin-Wagner theorem,[2] the Néel antiferromagnetic (AF) long-range order in 2D can exist only at zero temperature, but even then it can still be reduced by quantum fluctuations. It has been established that at $T=0$ the AF order survives for several lattices, such as for the square lattice. The ordered ground state is accompanied by gapless low-energy excitations, which, according to spin-wave theory[3] and the nonlinear σ-model description,[4] behave as

$$\Delta E_q \sim L^{-z_q}, \quad z_q = 2, \tag{1}$$

where L is the linear size of the system, z_q is the dynamical exponent, and the subscript q refers to quantum fluctuations. The AF order in the ground state can be suppressed by introducing frustration (e.g., with diagonal couplings in the square lattice: the J_1-J_2 model),[5] by dimerizing the lattice,[6] or by coupling two square lattices to form a bilayer.[7–9] By increasing these disordering effects, the AF order is reduced progressively and will disappear at an order-disorder quantum phase transition point.

In real materials impurities and other types of quenched disorder are inevitably present or can be controlled by doping. Fluctuations due to quenched disorder can further destabilize the AF order, resulting in disordered ground states and random quantum critical points. Quasi-two-dimensional materials, such as La_2CuO_4 doped with Mg (or Zn) and K_2CuF_4 (or K_2MnF_4) doped with Mg, can be approximately described by the 2D AF Heisenberg model with static nonmagnetic impurities. In these systems a disorder-induced quantum phase transition from Néel order to a disordered spin-liquid phase was observed.[10]

Theoretical investigations of the disorder effects in 2D Heisenberg antiferromagnets have been mainly restricted to dilution effects. Quantum Monte Carlo (QMC) simulations of the diluted square-lattice model showed that the AF long-range order persists up to the classical percolation point and the critical exponents are identical to those of classical percolation for all S.[11] In studies of the square-lattice model with staggered dimers and dimer dilution, unusual critical properties were found; among others, at the classical (bond) percolation point there is a critical line with varying exponents.[12] In the 2D bilayer Heisenberg antiferromagnet the random dimer dilution can be introduced by randomly removing the interlayer bonds. In recent QMC simulations,[13–15] random quantum critical points with a universal dynamical exponent $z \approx 1.3$ were deduced by varying the ratio of the interlayer and intralayer couplings below the percolation threshold.

In the presence of bond randomness, the low-energy properties of the above-mentioned 2D random models can be studied by a strong-disorder renormalization group (RG) approach,[16] which was originally introduced by Ma, Dasgupta, and Hu[17] for the 1D random AF Heisenberg model. In a detailed analysis of this RG procedure Fisher[18] solved the RG equations for the 1D model analytically and showed that during renormalization the distribution of the couplings broadens without limit, indicating that the RG flow goes to

an infinite-randomness fixed point.[19] Due to infinite randomness, approximations in the RG procedure are negligible and the scaling behavior of the system—in both a dynamical and static sense—is asymptotically exact. The ground state of the 1D model, the so-called random singlet state,[20] consists of effective singlet pairs and the two spins in a given singlet pair can be arbitrarily far from each other. Renormalization of the 1D model with enforced dimerization (with different probability distributions of the even and odd couplings) leads to a random dimer phase,[21] which is a prototype of a quantum Griffiths phase. The singular properties of the Griffiths phase are controlled by a line of strong-disorder fixed points; along this line, the disorder-induced dynamical exponent z varies continuously with the strength of dimerization. The dynamical exponent, calculated by the RG method, is presumably asymptotically exact; however, the static behavior, such as the density profiles, is correct only up to the correlation length in the system.

Variants of the strong-disorder RG method have been applied for various 1D and quasi-1D (spin ladder) random Heisenberg models. In Heisenberg models with mixed ferromagnetic and antiferromagnetic couplings,[22] during renormalization large spins are formed and the dynamical properties of these large-spin phases are different from the Griffith phases; for example, the uniform magnetic susceptibility has a Curie-like low-temperature behavior. The strong-disorder RG method for more complicated geometries, such as in 2D, can only be implemented numerically and the calculated dynamical exponent z is presumably approximate. However, we expect that the qualitative form of the low-energy singularities is correctly predicted by these investigations. In previous studies[23] 2D and 3D Heisenberg antiferromagnets with and without frustration in the presence of bond disorder were numerically studied for random coupling constants taken from the Gaussian or from the boxlike distributions. In contrast to the 1D case, no infinite-disorder fixed point is observed. Nonfrustrated models are shown to have a conventional Griffiths-like random fixed point, whereas the dynamical singularities of frustrated models are controlled by large-spin fixed points.

In the present paper we extend previous investigations of 2D random Heisenberg models in different directions. First, we consider the strong disorder represented by a power-law distribution of the couplings and study systematically the variation of the dynamical singularities with the strength of the bond disorder. In particular, we are interested in the localization properties of the low-energy excitations. Second, we consider nonmagnetic impurities and study the combined effect of bond disorder and site dilution. Our third direction of study considers AF bilayers with bond disorder and randomly removed interlayer dimers. Evidently, with vanishing interlayer coupling this problem reduces to our second model.

The paper is organized as follows. The models under investigation as well as their basic properties are presented in Sec. II. The strong-disorder RG method and the properties of the basic fixed points are shown in Sec. III. A description of the QMC stochastic series expansion method, which is used to support the strong-disorder RG approach, is given in Sec. IV. Results of the critical properties as well as the Griffiths
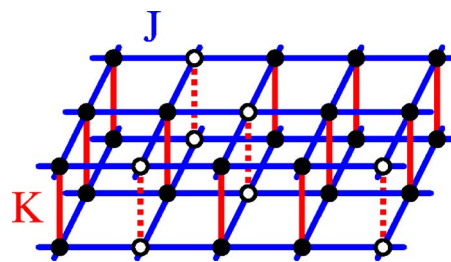

FIG. 1. (Color online) The diluted bilayer model. Solid circles represent spins, and open circles indicate the removed dimers. Neighboring spins in each plane interact with the coupling J, and the interplane coupling is K.

singularities of different disordered Heisenberg AF models are presented in Sec. V and discussed in Sec. VI.

II. MODELS AND PHASE DIAGRAMS

We start with the definition of the most general model considered in this paper: the double-layer Heisenberg antiferromagnet with random dimer dilution (see Fig. 1) which is described by the Hamiltonian

$$\mathcal{H} = \sum_{n=1,2} \sum_{\langle i,j \rangle} J_{i,j} \epsilon_i \epsilon_j \mathbf{S}_{i,n} \cdot \mathbf{S}_{j,n} + \sum_i K_i \epsilon_i \mathbf{S}_{i,1} \cdot \mathbf{S}_{i,2}. \quad (2)$$

Here $\mathbf{S}_{i,n}$ is a spin-1/2 operator at site i of the nth square lattice layer. The antiferromagnetic planar (interlayer) coupling constants $J_{i,j}$ (K_i) are independently and identically distributed random variables. The dimer dilution at site i is represented by the variable ϵ_i, which is $\epsilon_i=0$ with probability p and $\epsilon_i=1$ with probability $1-p$.

To our knowledge, this model has so far only been studied without bond disorder—i.e., $K_i \equiv K \; \forall i$ and $J_{i,j} \equiv J \; \forall i,j$. The schematic phase diagram of this model at zero temperature in terms of the coupling ratio $g \equiv K/J$ and dilution p is shown in the plane $D=0$ in Fig. 2. The point at $(g=0, p=0)$ corresponds to two uncoupled nondiluted square-lattice AF Heisenberg model and exhibits AF long-range order in its ground state.[24] At $p=0$ a finite interplane coupling, $g>0$, causes a tendency for neighboring spins in the adjacent layers to form singlets and the AF order is therefore reduced. If the coupling ratio exceeds some critical value, $g>g_c$, the system will undergo a quantum phase transition from an AF state to a disordered state. This $T=0$ order-disorder transition is expected to belong to the universality class of the 3D classical Heisenberg model according to the σ-model description by Chakravarty *et al.*[4] Results of recent QMC simulations are in accordance with this conjecture, and the critical ratio is calculated as $g_c \approx 2.5220$.[9,25]

Along the horizontal axis of Fig. 2—i.e., with $g=0$ (and $D=0$)—we have two uncoupled site-diluted Heisenberg AF planes. Increasing dilution suppresses AF order progressively and according to QMC results the quantum phase transition takes place at the classical site-percolation threshold,[26] $p_p=0.407$. Furthermore, the critical exponents are those of the classical percolation transition.[13] Now having both dilution, $p>0$, and finite interlayer coupling, $g>0$, the phase boundary $g_c(p)$ is monotonically decreasing with increasing
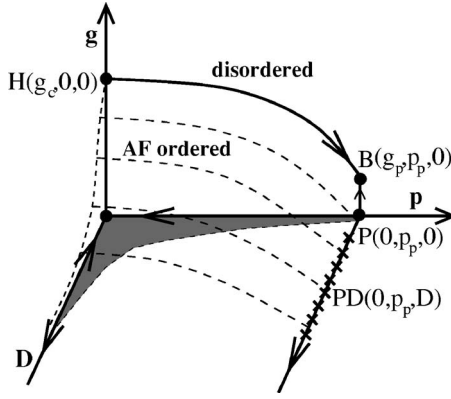
FIG. 2. Schematic phase diagram of the dimer diluted bilayer Heisenberg antiferromagnet, as a function of the coupling ratio g, the fraction of the removed interplane dimers p, and the strength of the bond disorder D. The disordered phase and the AF ordered phase are separated by a critical surface, indicated by dashed lines, which is located at $p \leq p_p$ and $g_c(p,D)$, where p_p is the site-percolation threshold. In the model without bond disorder, $D=0$, there are two unstable fixed points, H and P, as well as a stable bilayer fixed point B. In the diluted single layer $g=0$ with bond disorder, the phase boundary is located at the percolation threshold with universal static and strong-disorder-dependent dynamical critical exponents, indicated by the line of fixed points PD. In the AF-ordered phase the dynamical exponent z is determined by quantum fluctuations for weak disorder (indicated by a gray region at $g=0$), whereas z is D dependent for strong disorder.

dilution.[13,14] However, even at the percolation threshold there is a finite critical coupling: $g_c(p_p) \equiv g_p \approx 0.16$, and this fixed point, marked by B in Fig. 2, is found to control the phase transition between the ordered and disordered phases for $p > 0$ and $g > 0$.[13,14] This fixed point is a conventional random fixed point with power-law dynamical scaling and universal exponents.[15]

In this paper we extend the space of parameters by introducing bond disorder, such that the intralayer and interlayer couplings are independent and identically distributed random variables taken from the distributions

$$\pi(J) = \frac{J_{\max}^{-1/D}}{D} J^{-1+1/D}, \quad \text{for } 0 < J \leq J_{\max},$$

$$\rho(K) = \frac{K_{\max}^{-1/D}}{D} K^{-1+1/D}, \quad \text{for } 0 < K \leq K_{\max}, \quad (3)$$

respectively. Here $D^2 = \text{var}[\ln J] = \text{var}[\ln K]$ measures the strength of disorder ($\text{var}[x]$ stands for the variance of x) and the control parameter is defined as $g = K_{\max}/J_{\max}$. Note that a uniform distribution corresponds to $D=1$. In particular we are interested in the properties of the phase diagram and the singularities at the phase transitions as well as the form of disorder-induced low-energy excitations in the different regions.

III. STRONG-DISORDER RG METHOD AND ITS FIXED POINTS

The strong-disorder RG method[16] is an important tool to study random quantum systems. Here we recapitulate the basic ingredients of the method used for the 2D random Heisenberg antiferromagnet.

The RG proceeds by eliminating at each step a term in the Hamiltonian with the largest gap separating the ground state and the first excited state. This decimation process generates effective couplings between the remaining sites which are calculated perturbatively. For a lattice with more complex structure than a single chain, such as the bilayer antiferromagnet, the renormalized Hamiltonian contains effective spins of arbitrary size with a complicated correlated network and has both antiferromagnetic and ferromagnetic (F) couplings. The RG procedure for this Hamiltonian thus consists of two types of decimation rules, one for singlet formation (for equal-size spins with an AF bond), and one for cluster formation (for all other cases). Further details of the RG procedure can be found in Refs. 22, 23, and 27.

As the RG procedure is iterated, the cutoff of the energy gaps, denoted by Ω, is gradually decreased. In the vicinity of the low-energy fixed point $\Omega^* \to 0$, the low-energy tail of the distribution of the gaps for a large finite system of linear size L follows the relation

$$P(\Delta, \Omega, L) = L^z \widetilde{P}\left(\frac{\Delta}{\Omega}, \frac{L^{-z}}{\Omega}\right) \sim L^z \left(\frac{\Delta}{\Omega}\right)^\omega \sim L^{z(1+\omega)} \Delta^\omega, \quad (4)$$

which defines the gap exponent ω. The energy scale and length scale are related by $\Omega \sim L^{-z}$ with the disorder-induced dynamical exponent z. Note that with the initial power-law distribution of the couplings in Eq. (3) the initial gap exponent is given by $\omega_0 = -1 + 1/D$. At a conventional random fixed point, we have $\omega/\omega_0 = O(1)$, while at an infinite-disorder fixed point the distribution of the effective gaps broadens without limit, indicating $\omega/\omega_0 \to \infty$. If the low-energy excitations are localized, then the gap distribution for a fixed Δ is proportional to the volume of the system: $P(\Delta, \Omega, L) \sim L^d$. From Eq. (4), we obtain, in this case,

$$z = z' \equiv \frac{d}{1+\omega}; \quad (5)$$

here, an exponent z' is defined. Note that at an infinite-disorder fixed point the dynamical exponent z is formally infinite.

Another characteristic feature of the fixed point is the typical size of the effective cluster moment, $S_{\text{eff}} = |\Sigma_i \pm S_i|$, which is determined by the classical correlation of the spins in the ground state, and the positive (negative) sign corresponds to an F (AF) coupling. S_{eff} is expected to scale as $S_{\text{eff}} \sim L^{d\zeta}$. There are two types of fixed points concerning the value of ζ: In some models the decimated spin pairs are typically singlets or the size of the effective spins has a saturated value, which yields $\zeta = 0$ in the low-energy limit; in some models, mainly with frustration, large effective spins are formed, and if ferromagnetic and antiferromagnetic couplings are uncorrelated, one obtains[22] $\zeta = 1/2$. This state is called the large-spin phase.

In the RG method static correlations can be measured by considering the staggered ground-state correlation function $C(r)$ between two spins at distance r. This is defined as

$$C(r) \equiv C_{ij} = \langle \eta_{ij} \mathbf{S}_i \cdot \mathbf{S}_j \rangle, \tag{6}$$

where $\eta_{ij} = (-1)^{x_i + y_i + x_j + y_j}$ and r is measured by one-norm distance (also known as the Manhattan distance): $r = r_{ij} \equiv |x_i - x_j| + |y_i - y_j|$. This choice was made for computational convenience; in the limit $r \to \infty$, it yields the same asymptotic behavior of $C(r)$ as the one calculated with the Euclidean distance $r = \sqrt{(x_i - x_j)^2 + (y_i - y_j)^2}$. In our RG scheme, the correlations of spin pairs, which form an effective spin at each RG stage, are calculated by

$$\langle \mathbf{S}_i \cdot \mathbf{S}_j \rangle = \alpha_{ik} \alpha_{jl} \langle \mathbf{S}_k^{\text{eff}} \cdot \mathbf{S}_l^{\text{eff}} \rangle, \tag{7}$$

where $\alpha_{ik(jl)} = \langle \mathbf{S}_{i(j)} \cdot \mathbf{S}_{k(l)}^{\text{eff}} \rangle / \langle \mathbf{S}_{k(l)}^{\text{eff}\,2} \rangle$ are the proportionality coefficients for each spin. We assume zero correlation between two spins that do not form an effective spin. After accumulating the correlations between all decimated spin pairs, we divide the correlation for a given distance r by $2rL^2$, which corresponds to the number of pairs a one-norm distance r apart. Here we note that the RG results for static correlations are expected to be valid only in the vicinity of a (static) critical point. Thus the calculated correlation functions for the 2D problem are asymptotically correct only in the vicinity of the phase boundary. As reported for the 1D case,[28] the RG method underestimates the correlations, but provides quantitatively reliable decay behavior, which can be used to estimate the exponent of the power-law decay of the correlations at the phase boundary.

Within the RG study, thermodynamics can be understood by stopping the RG procedure when the energy scale—i.e., the cutoff of energy gaps Ω in our case—reaches the thermal energy at a given temperature T.[18,20] At this scale, almost all decimated spins are effectively frozen, while almost all remaining spins involve couplings which are much less than T and hence can be regarded as free. The magnetic susceptibility per spin is then mainly given by the Curie contribution of those remaining spins and is given by

$$\chi(T) \sim \frac{1}{TL^d} \sum_i^{n_T} S_i(S_i + 1), \tag{8}$$

where the summation runs over all clusters left at the given temperature T and S_i is the (effective) spin moment. In the low-temperature limit the susceptibility generally behaves as a power law:

$$\chi(T) \sim T^{-\theta}. \tag{9}$$

If during renormalization there is no large-spin formation—i.e., $\zeta = 0$—then $\theta = \omega$ in the low-T limit, whereas in the large-spin phase with $\zeta = 1/2$ there is a Curie-like dependence: $\theta = 1$. Singularities of the specific heat or the magnetization can be calculated similarly; see Ref. 16.

IV. QUANTUM MONTE CARLO METHOD

A. Description of the method

Here we use the QMC stochastic series expansion (SSE) method within a directed loop framework introduced by Syljuåsen and Sandvik in Ref. 29. Starting with a general Heisenberg Hamiltonian with random exchanges $J(b)$, we can rewrite it as a sum over diagonal and off-diagonal operators:

$$\mathcal{H} = -\sum_{b=1}^{N_b} J(b)[H_{1,b} - H_{2,b}], \tag{10}$$

where b denotes a bond connecting a pair of interacting spins $(i(b), j(b))$, N_b is the total number of bonds,

$$H_{1,b} = C - S_{i(b)}^z S_{j(b)}^z \tag{11}$$

is the diagonal part, and the off-diagonal part is given by

$$H_{1,b} = \frac{1}{2}[S_{i(b)}^+ S_{j(b)}^- + S_{i(b)}^- S_{j(b)}^+] \tag{12}$$

in the basis $\{|\alpha\rangle\} = \{|S_1^z, S_2^z, \ldots, S_L^z\rangle\}$. The constant C which has been added to the diagonal part ensures that all nonvanishing matrix elements are positive. The SSE algorithm consists in Taylor expanding the partition function $Z = \text{Tr}\{e^{-\beta\mathcal{H}}\}$ up to some power $\mathcal{M}$ which is adapted during the simulations in order to ensure that all the elements of order higher than $\mathcal{M}$ in the expansion do not contribute. So

$$Z = \sum_\alpha \sum_{S_\mathcal{M}} \frac{\beta^n (\mathcal{M} - n)!}{\mathcal{M}!} \left\langle \alpha \left| \prod_{i=1}^{\mathcal{M}} J(b_i) H_{a_i, b_i} \right| \alpha \right\rangle, \tag{13}$$

where $S_\mathcal{M}$ denotes a sequence of operator indices,

$$S_\mathcal{M} = [a_1, b_1], [a_2, b_2], \ldots, [a_\mathcal{M}, b_\mathcal{M}], \tag{14}$$

with $a_i = 1, 2$, corresponds to the type of operator (diagonal or not) and $b_i = 1, 2, \ldots, N_b$ is the bond index. A Monte Carlo configuration is therefore defined by a state $|\alpha\rangle$ and a sequence $S_\mathcal{M}$. Of course, a given operator string does not contain $\mathcal{M}$ operators of type 1 or 2, but only n; so in order to keep constant the size of $S_\mathcal{M}$, $\mathcal{M} - n$ unit operators $H_{0,0} = 1$ have been inserted in the string, taking into account all the possible ways of insertions. The starting point of a simulation is given by a random initial state $|\alpha\rangle$ and an operator string containing $\mathcal{M}$ unit operators $[0,0]_1, \ldots, [0,0]_\mathcal{M}$. The first step is the *diagonal update* which consists in exchanging unit and diagonal operators at each position p $[0,0]_p \leftrightarrow [1, b_i]_p$ in $S_\mathcal{M}$ with Metropolis acceptance probabilities

$$P_{[0,0]_p \to [1,b]_p} = \min\left(1, \frac{J(b) N_b \beta \langle \alpha(p)|H_{1,b}|\alpha(p)\rangle}{\mathcal{M} - n}\right), \tag{15}$$

$$P_{[1,b]_p \to [0,0]_p} = \min\left(1, \frac{\mathcal{M} - n + 1}{J(b) N_b \beta \langle \alpha(p)|H_{1,b}|\alpha(p)\rangle}\right). \tag{16}$$

During the "propagation" from $p = 1$ to $p = \mathcal{M}$, the "propagated" state

$$|\alpha(p)\rangle \sim \prod_{i=1}^{p} H_{a_i,b_i}|\alpha\rangle \qquad (17)$$

is used and the number of nonunit operators n can vary at each index p. The following step is the *off-diagonal update*, also called the *loop update*, carried out at n fixed. Its purpose is to substitute $[1,b_i]_p \leftrightarrow [2,b_i]_p$ in a nonlocal manner but in a cluster-type update. At the SU(2) AF point, the algorithm is deterministic because one can build all the loops in a single way.[29] One MC step is composed of one *diagonal* and *off-diagonal* updates. Measurement of physical observables is started after a suitable number of equilibration steps in which also $\mathcal{M}$ is adapted.

B. Monte Carlo measurement issues

The precise determination of physical observables using QMC simulations suffers obviously from statistical errors since the number of MC steps is finite. As we deal with disordered spin systems, fluctuations between different realizations of the disorder are another source of errors. However, one can use a relatively small number of MC steps for each disorder realization (typically ~ 100 at each temperature) since for the strong disorders considered here, the variation between different realizations produces larger error bars than statistical errors. Then we need to perform a disordered-samples average over a significant number of realization: typically we use 10^3 realizations.

In order to study the low-temperature properties, we use the β-doubling strategy introduced by Sandvik[11] to accelerate the cooling of the system during a QMC simulation. Such a scheme is a very powerful tool because it allows one to reach extremely low temperatures rather rapidly *and* reduces considerably equilibration times in the MC simulation. The procedure is quite simple to implement, and its basic ingredient consists in carrying out simulations at successive inverse temperatures $\beta_n = 2^n$, $n = 0,1,\ldots,n_{max}$. Starting with a given disorder realization at $n = 0$ we perform a small number of equilibration steps, N_{eq}, followed by $N_m = 2N_{eq}$ measurement steps. At the end of the measurement process, β is doubled (i.e., $n \rightarrow n+1$), and in order to start with an "almost equilibrated" MC configuration, the starting sequence used is the previous $S_\mathcal{M}$ doubled—i.e.,

$$S_{2\mathcal{M}} = [a_1,b_1],\ldots,[a_\mathcal{M},b_\mathcal{M}][a_\mathcal{M},b_\mathcal{M}],\ldots,[a_1,b_1]. \qquad (18)$$

V. NUMERICAL RESULTS

In practice we started with a finite system of linear size L (up to $L=64$) with periodic boundary conditions for each single layer and decimated the bonds and spins successively by the RG procedure until there is only one effective spin cluster (or one spin singlet) surviving. The static characteristics of the system, in particular in the vicinity of the phase boundaries, can be deduced from the average spin-spin correlation function. On the other hand, the form of the dynamical singularities can be obtained from the temperature dependence of the uniform susceptibility and from the distribution of the first energy gaps corresponding to the energy scale of the last decimation step. From the histogram of the gaps we have extracted the gap exponent ω and the dynamical exponent z, as discussed in Sec. III. Depending on the size of the system we have considered 1000–10 000 disorder realizations.

For the single layer we also compare the RG results with QMC simulations performed at finite temperature on 32×32 square lattices and averaged over 1000 disorder realizations.

In what follows, we present the phase diagram of the system and the properties of the different bond-randomness-driven phase transitions. The dynamical properties of the ordered and disordered phases are discussed afterwards.

A. Phase diagram and critical properties

Our main results are summarized in the schematic phase diagram of the system depicted in Fig. 2. It contains two phases: the ordered AF phase and the disordered paramagnetic phase. The phase transition between these two phases is controlled by several fixed points as shown in the phase diagram. The fixed points located at $D=0$, denoted by H, B, and P in Fig. 2, had already been carefully studied by QMC simulations.[9,13–15] The measured critical exponents at these fixed points are shown in Table I, along with the results for $D>0$ obtained from our study.

We first consider the fixed points (PD) at the percolation threshold $p=p_p$ for $g=0$. Figure 3 shows the average spin-spin correlation function $C_{av}(r)$ at $g=0$ for different dilution p and for strong bond randomness, $D=3$ ($D=10$). From $p < p_p$ to $p > p_p$ the decay of $C_{av}(r)$ in the log-log plot changes from an upward to a downward curvature; the decay of $C_{av}(r)$ does not show significant differences between $D=3$ and $D=10$. The lack of monotonicity in $C(r)$ for $p=0.125$ and $p=0.33$, far below p_p, observed in Fig. 3 may be caused by the fact, as pointed out before, that the application of the RG method for calculating correlation functions is reliable only near the phase transition, where the correlation length is large. To have a closer look at the vicinity of the percolation

TABLE I. Critical exponents at the fixed points of the bilayer Heisenberg antiferromagnet with random dimer dilution and bond disorder; see Fig. 2. H: nonrandom bilayer (classical 3D Heisenberg model) (Ref. 30). P: diluted single layer (classical 2D percolation) (Ref. 31). $0B$: dimer diluted bilayer (Ref. 15). PD: diluted single layer with bond disorder. In the last rows critical exponents measured at two general points of the critical surface are presented.

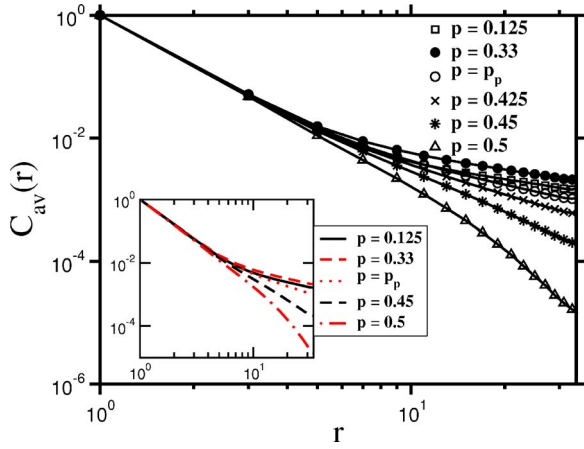| Fixed point	Position (g,p,D)	β/ν	z	ν
H (Ref. 30)	$(g_c,0,0)$	0.51	1	0.70
P (Ref. 31)	$(0,p_p,0)$	5/48	91/48	4/3
B (Ref. 15)	$(g_p,p_p,0)$	0.56	1.31	1.16
PD	$(0,p_p,D>0)$	0.50	$\sim 3.2D$	
	$(1.2,0.33,0.7)$	0.56	1.36	
	$(7.5\times10^{-4},0.33,3)$	0.80	5.13	

FIG. 3. (Color online) Log-log plot of the average spin-spin correlation function at $g=0$ measured for a $L=64$ lattice with bond randomness $D=3$ and $D=10$ (inset) for different site dilutions p. The data are scaled to unity at $r=1$. For $p>p_p$ the curves show downward curvature, indicating a faster decay than a power law characteristic of the disordered phase, while for $p<p_p$ the curves bend upward.

threshold, we have calculated the correlation functions $C_{av}(L/2)$ for different system sizes, as shown in Fig. 4. Considering the systematic underestimation of the correlations by the RG scheme that we use, we have not deduced the staggered magnetization from the extrapolations of $C_{av}(L/2)$; nevertheless, the decay behavior of $C_{av}(L/2)$ implies that the order-disorder transition point p^* may occur close to the percolation threshold p_p. Indeed the algebraic decay $C_{av}(L)$ $\sim L^{-2\beta/\nu}$ at $p=p_p$ indicates a reasonable scenario that the transition point p^* coincides with the percolation threshold p_p, as suggested by accurate QMC studies by Sandvik[11] for the $D=0$ case. The estimated decay exponent $2\beta/\nu$ $=1.01(7)$ is found to be the same for stronger disorder with $D=10$; see the inset of Fig. 4. Note that this decay exponent
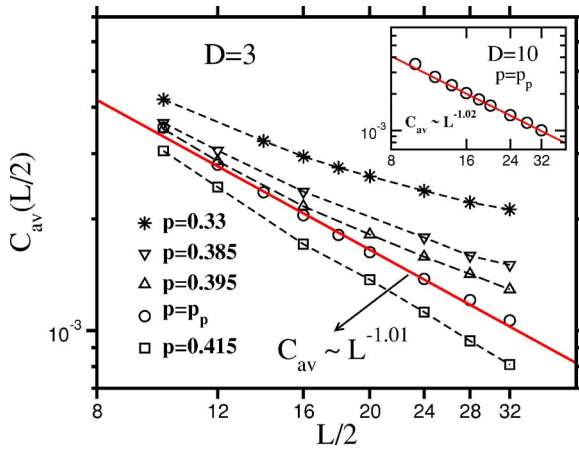

FIG. 4. (Color online) A plot of the average spin-spin correlation function for different system sizes L near the percolation threshold $p=p_p$ for $D=3$. The power-law decay at $p=p_p$ gives the decay exponent $2\beta/\nu=1.01$, as indicated by the solid line. The inset shows the correlation for $D=10$ at $p=p_p$ with the decay exponent $2\beta/\nu=1.02$.
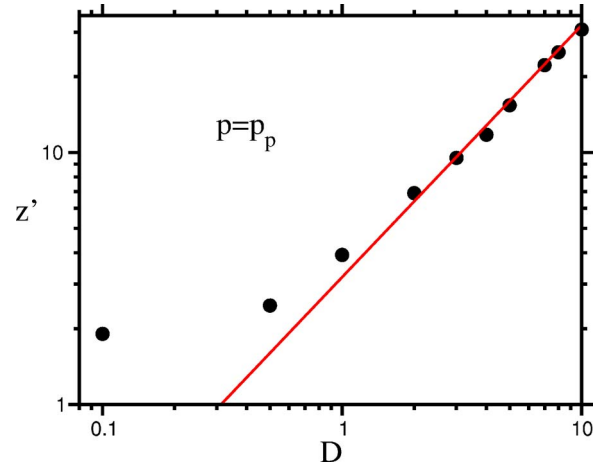

FIG. 5. (Color online) Disorder dependence of the z' exponent at the percolation threshold (at the line of fixed points PD in Table I) in a log-log plot. The slope of the straight line is unity.

is much larger than $2\beta/\nu=0.21$ for $D=0$. From this, one might suspect that the percolating cluster is no longer ordered in the presence of strong bond randomness.[32] To decide unambitiously whether AF long-range order persists up to p_p also for $D>0$ and whether the percolating cluster is ordered, a careful MC study along the lines of Ref. 11 is definitely warranted.[33] For $p=p_p$, we have also studied the dynamical exponents. Unlike the decay exponent of $C_{av}(r)$, which is D independent, the dynamical exponent z' obtained from the slope of the gap distribution is found to depend linearly on the strength of the disorder in the large D region: $z'\approx3.2D$, as shown in Fig. 5. For weak bond disorder D <1, instead, we find that z' approaches the value $z=91/48$ for the $D=0$ case.

Now we turn to the phase boundary for finite bilayer coupling $g>0$. At a given $p<p_p$ and a fixed D, we calculated the average spin-spin correlations $C_{av}(r)$ for different values of the bilayer coupling g. As illustrated in Fig. 6 for p $=0.33$, we find that the decay behavior of $C_{av}(r)$ changes its characteristic from the one for the AF-ordered phase to the one for the disordered phase as a critical value of g_c is traversed. For weak bond disorder $D=0.7$, the critical coupling is located around $g_c=1.2$ and we note that the decay exponent of the critical correlation, $2\beta/\nu\approx1.12$, is approximately the same as for $D=0$. For strong bond disorder $D=3$, the phase boundary shifts to a very small value of g_c $\approx0.000\,75$ with the critical exponent $2\beta/\nu\approx1.6$. The extremely small value of g_c, which decreases even with D, makes the investigation of the D dependence of the critical exponents difficult. From our results for $C_{av}(r)$ up to $D=5$, the decay exponent β/ν appears to be D independent for a given p in the strong-disorder regime, while it varies with the dilution p. To locate the critical bilayer coupling g_c we also made use of the results for the dynamical exponent z'; cf. Fig. 7 for $p=0$, $p=0.125$ and 0.33. As g is increased, the dynamical exponent is approximately independent of the value of g, but jumps to another g-independent value around the transition point. For weak bond disorder, such as D $=0.7$ for $p=0.33$, we find $z'\approx1.36$, which is close to the
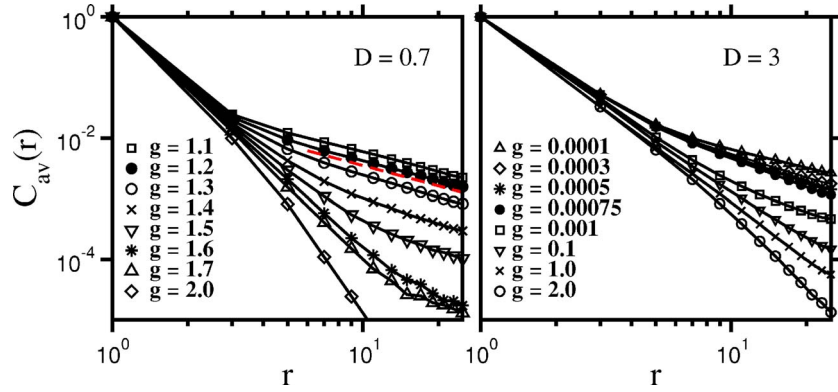
FIG. 6. (Color online) The in-plane average spin-spin correlations of the double-layer AF model versus r in log-log plots for bond randomness $D=0.7$ (left) and $D=3$ (right) for different values of the bilayer coupling at $p=0.33$ for $L=48$. The data are scaled to unity at $r=1$. We observe a crossover from an upward curvature through a power-law decay to a downward curvature. The order-disorder transition point $g_c \approx 1.2$ shows an asymptotically linear dependence in the large-r regime with a slope $2\beta/\nu \approx 1.12(4)$ (indicated by a dashed line) which is approximately the same as for $g=0$. For $D=3$ the transition point shifts to a very small value of $g_c=0.000\,75$ and the critical exponent is estimated as $2\beta/\nu \approx 1.60(4)$.

value found for the case without bond disorder.[15] For strong disorder, in which case the RG approach is expected to be more appropriate, the dynamical exponent increases with D, which is a tendency already noticed for $g=0$.

To summarize our numerical findings we indicate two different regimes of the phase transition. For *weak bond disorder* the static critical exponent β/ν as well as the dynamical exponent z' seems to coincide with the values for the case without bond disorder. For *strong bond disorder* the critical coupling g_c is reduced to a very small value and the static exponent approaches a D-independent, but dilution-dependent value, whereas the dynamical exponent at the transition point depends (linearly) on the strength of the bond randomness. The position of the order-disorder transition for a single layer (corresponding to $g=0$) is located at the percolation threshold. Along the line of *PD* fixed points, the exponent β/ν deviates from the value for $D=0$, but seems to
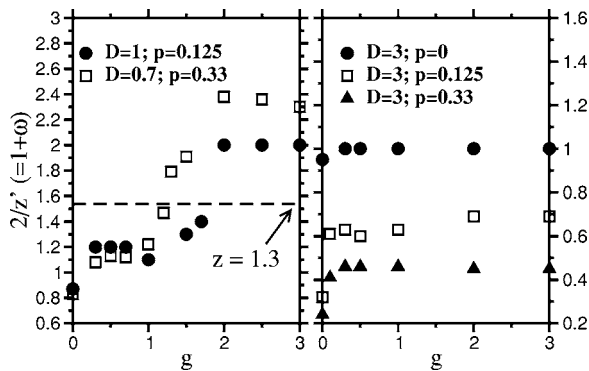

FIG. 7. Variation of the gap exponent with the coupling ratio g for weaker (left) and stronger (right) bond disorder for different values of the dimer dilution. Note that in the ordered phase $g<g_c$ as well as in the disordered phase $g>g_c$, z' is approximately independent of g. For weaker bond disorder there is a jump at the transition point $g=g_c$ and the dynamical exponent is close to the value $z(g_c) \approx 1.3$ at the fixed point B for $D=0$ case, which is denoted by a dashed line. For strong disorder (right) the transition point is located at a very small g so that it cannot be identified in the figure.

be D independent, while the dynamical exponent exhibits a linear dependence on D in the large-D limit.

B. Griffiths singularities in the ordered phase

As discussed in the preceding subsection, the random dimer diluted bilayer antiferromagnet exhibits AF order, provided $p<p^*$ and the bilayer coupling is sufficiently small. The order-disorder transition point $p=p^*$ appears to agree with $p=p_p$. The low-energy fixed points governing the Griffiths singularities in the ordered phase are of different types in the specific regions. These fixed points are in turn an effective singlet for $p=0$ and $g=0$ (single layer without site dilution), a large-spin fixed point for $0<p<p_p$ and $g=0$ (single layer with site dilution), and an effective singlet for $0<p<p_c$ and $0<g<g_c$ (bilayer with dimer dilution). In the following we study these different cases separately.

1. Two-dimensional undoped antiferromagnet

We start by discussing the results for the two-dimensional random Heisenberg model, which corresponds to $g=0$ and $p=0$. A recent numerical study[34] suggested that the AF order in this region vanishes only in the limit of infinite bond randomness. In our preliminary study[23] we showed that the low-energy fixed point of the model is conventional; however, the dependence on the strength of disorder was not investigated extensively. Here we calculate the gap exponent ω and the related exponent z' defined in Eq. (5), as well as the dynamical exponent z, as a function of the disorder strength D. The gap exponent ω is obtained from the slope of the distribution of the log gaps in the small-gap limit, whereas the dynamical exponent is determined from the optimal scaling collapse of the curves according to Eq. (4) as illustrated in Fig. 8. For localized excitations the scaling curve is conjectured[35] from extreme-value statistics to be described by the Fréchet distribution[36]

$$\tilde{P}_1(u) = \frac{d}{z}u^{d/z-1}\exp(-u^{d/z}), \qquad (19)$$

with $d=2$ and $u=u_0 L^z \Delta$, where u_0 is a nonuniversal constant.
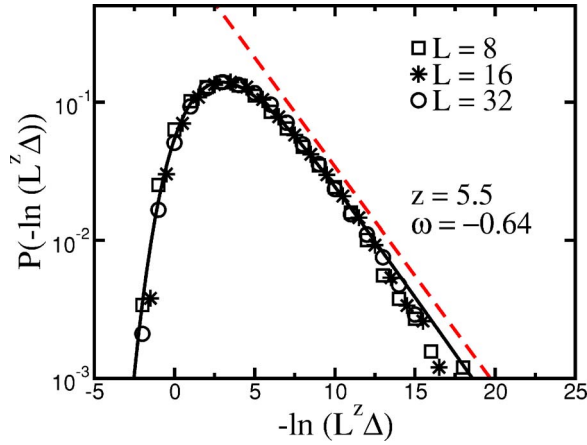
FIG. 8. (Color online) A scaling plot of the log-energy gaps for the 2D antiferromagnet with strong bond randomness $D=8$ obtained from 10 000 samples for each size. The gap exponent $\omega \approx -0.64$ follows from the slope at small energy gaps, and the dynamical exponent $z \approx 5.5$ is determined by the fit parameter in Eq. (4). Note that the relation in Eq. (5) is satisfied, implying that the low-energy excitations are localized. The solid line represents the Fréchet distribution given in Eq. (19).

Both z and z' have an approximately linear D dependence in the strong-disorder region ($D \geq 3$) as shown in Fig. 9, while no significant disorder dependence ($\omega \approx 0.7$) is found for weak disorder.[23] The exponents z and z' are found to be identical only for quite strong disorder $D \geq 7$. This indicates that the low-energy excitations are localized only in the strong-disorder regime.

We note that the vanishing energy gaps calculated by the RG approach are solely induced by disorder. However, quantum fluctuations also induce vanishing gaps which are characterized by a dynamical exponent $z_q = 2$; see Eq. (1). The true dynamical exponent is then given by $z_{\text{true}} = \max\{z_q, z\}$, so that $z_{\text{true}} = z_q = 2$ for weak randomness $D < 3$.

We have also calculated the uniform magnetic susceptibility as a function of the temperature, which is shown in Fig. 10 for different disorder strengths. Both RG and QMC re-
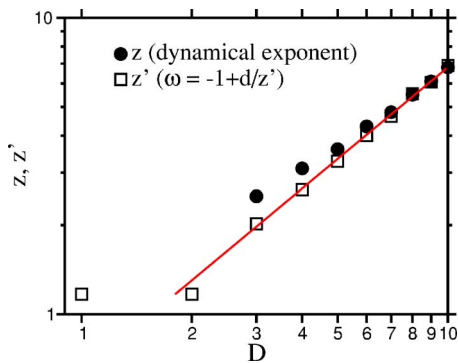

FIG. 9. (Color online) Variation of the disorder-induced dynamical exponent z and the exponent z' with the bond randomness strength D at $g=0$ and $p=0$ in a log-log plot. Note that the dependence for $D \geq 3$ is approximately linear and the values of z and z' fit well for $D \geq 7$, indicating that the low-energy excitations are localized.

sults are shown, and they display an excellent agreement. For strong bond randomness, the low-T susceptibility exhibits a power-law temperature dependence as given in Eq. (9) and the exponent θ is disorder dependent (see Table II). The same behavior of the magnetic susceptibility has been found for the antiferromagnetic spin-1/2 ladders.[37] Note, however, that the QMC results, shown in the right panel of Fig. 10, display a slow saturation of χ when $T \to 0$ (at least for $D \leq 5$) which is not a finite-size effect[38] but a signature of a tendency towards Néel ordering at $T=0$.[34]

Finally, we note that effective spins with size larger than 1/2 are formed during the RG procedure because of the generation of F couplings. In the low-energy limit, the overall strength of the F couplings, however, becomes much weaker than that of the AF couplings, which leads to the disappearance of large effective spins and the singlet ground state. This agrees with the Marshall's theorem[39] which states that the ground state of a bipartite AF Hamiltonian with equal-size sublattices is a total spin singlet.

2. Two-dimensional antiferromagnet with site dilution

The low-energy behavior of the site-diluted Heisenberg antiferromagnet is controlled by a large-spin fixed point, which is different from the undoped case where the last decimated pair of spins is an effective singlet. The situation is similar to that of antiferromagnetic spin-1/2 ladders with random site dilution. In this case Sigrist and Furusaki[40] argued that if two vacancies are in the same sublattice, the ground state is no longer a singlet; thus, there are effective spins of size larger than 1/2. This has been verified by numerical strong-disorder RG calculations.[41] In the 2D site-diluted case we also observed in our numerical RG calculation that the energy gap associated with an effective F coupling may become the largest gap to be decimated at some stage of the RG, especially in the low-energy regime. This will then lead to the formation of large effective spins as described in Sec. III.

We calculated the average size of the effective spin at the last decimation step $\langle S_{\text{eff}} \rangle$ for various dilution concentrations ($p=0.125$ and 0.33 and at p_p) and system sizes L. In the ordered phase, below the percolation threshold, $p \leq p_p$, the average spin size is found to increase linearly with the system size:

$$\langle S_{\text{eff}} \rangle \sim L, \tag{20}$$

which is demonstrated in Fig. 11. This result agrees with the scenario for the large-spin phase, as discussed below Eq. (5). At the percolation threshold the same argument leads to $\langle S_{\text{eff}} \rangle \sim L^{d_f/2}$, with $d_f = 91/48$ being the fractal dimension of the percolation cluster.[31]

A hallmark of the large-spin phase is the universal temperature dependence of some thermodynamic quantities; in particular, the disorder-averaged uniform susceptibility given in Eq. (9) shows a Curie-like behavior at low temperatures. This is checked in Fig. 12 in which the susceptibility obtained from both RG and QMC simulations is plotted for different strengths of the bond randomness and dilution concentrations. For not too strong bond disorder the agreement with the Curie law is good, while for strong bond disorder
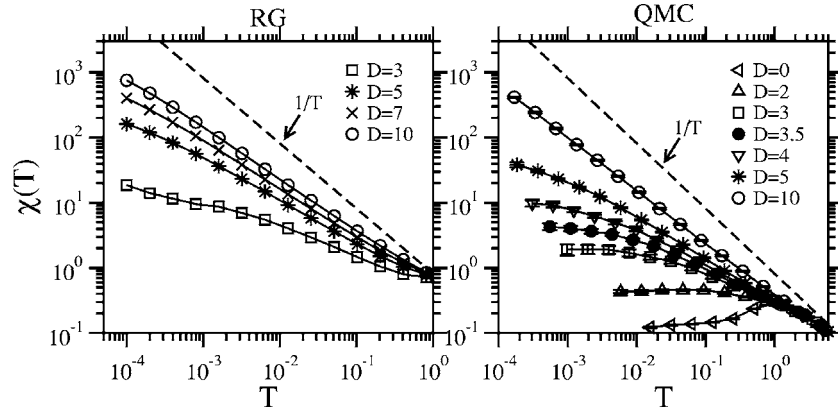
FIG. 10. Disorder average uniform susceptibility $\chi(T)$ as a function of temperature T for various disorder strengths D at $g=p=0$. Left panel: RG results. From the low-temperature regime ($T \lesssim 10^{-2}$) the exponent θ is estimated as $\theta=0.36$ for $D=3$, $\theta=0.60$ for $D=5$, $\theta=0.71$ for $D=7$, and $\theta=0.77$ for $D=10$. For all cases studied, the temperature dependence deviates from Curie-like $1/T$ behavior indicated by the dashed line. Right panel: QMC results obtained on systems of 32×32 spins. The exponent θ is estimated in a range of $T\in[T^*,1]$ as $\theta=0.37$ for $D=3$ ($T^*\simeq0.02$), $\theta=0.45$ for $D=3.5$ ($T^*\simeq0.01$), $\theta=0.52$ for $D=4$ ($T^*\simeq0.01$), $\theta=0.61$ for $D=5$ ($T^*\simeq0.002$), and $\theta=0.81$ for $D=10$ ($T^*\simeq0.0001$).

this agreement is observed only for very low temperatures. Note that in the undoped regime the susceptibility exponent θ is a continuous function of the disorder; see Fig. 10.

From the distributions of the low-lying energy gaps, we obtained the dynamical exponent z and the gap exponent ω. Unlike for the undoped model, the exponents z and $z'=2/(1+\omega)$ in general do not agree with each other for $0<p<p_p$, even in the regime of strong bond disorder. This indicates that low-energy excitations are not localized due to the formation of large spins. Figure 13 presents the exponent z' as a function of p for $D=3$ and $D=10$. For a given bond disorder, the exponent varies continuously with p in the ordered phase ($p<p_p$), while going approximately to a constant in the disordered phase ($p>p_p$). We remind the reader that to obtain the true dynamical exponent z_{true} one should also consider the effect of quantum fluctuations and thus $z_{\text{true}}=\max\{z_q,z\}$ in the ordered phase.

3. Double-layer Heisenberg antiferromagnet

In the presence of random bilayer couplings $g>0$, the low-energy properties of the ordered phase are controlled by an effective singlet, for both $p=0$ and $0<p<p_c$, which in turn is the same as for the single-layer undoped model; see Sec. V B 1. Indeed, we observed similar low-energy properties. The dynamical exponent z and the exponent z' are disorder dependent, but vary only weakly with the bilayer coupling g; see Fig. 7. z and z' are identical only for strong

TABLE II. Exponent θ of the divergence of the uniform susceptibility for various disorder strengths D for $p=g=0$. Comparison between RG and QMC estimates.

D	θ_{RG}	θ_{QMC}
3	0.36	0.37
5	0.60	0.61
10	0.77	0.81

enough disorder, when the low-energy excitations are expected to be localized. The average uniform susceptibility has a disorder-dependent low-temperature behavior, and the exponent θ corresponds to the gap exponent ω.

C. Griffiths singularities in the disordered phase

The disordered phase of the system is divided into two parts with different low-energy properties.

(i) Above the percolation threshold $p>p_p$ and $g=0$ the spins form only finite connected clusters. As a consequence the average effective spin has a finite value, as shown in Fig. 11 for $p=0.42$. Due to the unpaired spins in the isolated connected spin clusters, the average uniform susceptibility is Curie like (see Fig. 12 for $p=0.5$). The dynamical exponent z and the gap exponent ω depend approximately linearly on
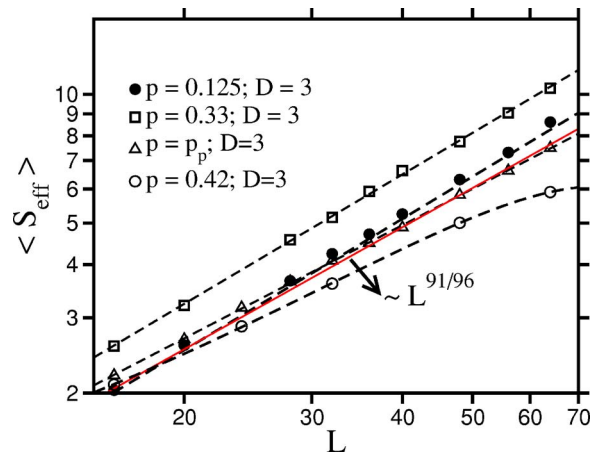

FIG. 11. (Color online) Variation of the disorder-averaged spin size $\langle S_{\text{eff}}\rangle$ with the linear system size L in a log-log plot for different site dilutions p at $D=3$ for the single-layer antiferromagnet $g=0$. For $p<p_p$ the spin size follows $\langle S_{\text{eff}}\rangle \sim L$, indicated by the dashed lines, whereas at $p=p_p$ the asymptotic power for large system sizes agrees with 91/96.
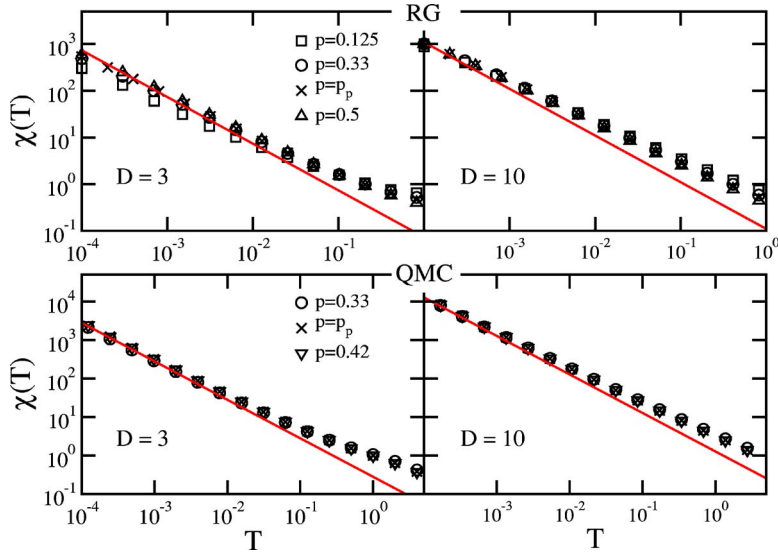
FIG. 12. (Color online) Temperature dependence of the uniform susceptibility per size for a diluted single layer, $g=0$, in log-log plots for various dilution concentrations p and for different bond random strength $D=3$ (left) and $D=10$ (right). The Curie-like $1/T$ behavior is indicated by straight lines. Both RG (upper panels) and QMC (lower panels) are shown.

the bond disorder D; they exhibit, however, no significant dependence on p, as shown in Fig. 13.

(ii) Above the critical bilayer coupling $g > g_c(p,D)$, the ground state is an effective singlet and in accordance with this the low-temperature uniform susceptibility is characterized by a nonuniversal exponent θ. For $p < p_p$, there is an infinite cluster and the low-energy physics is governed by rare finite regions which are locally ordered. The low-energy excitations connected to these regions are thus expected to be localized, provided the bond disorder is sufficiently strong. This is illustrated in Fig. 14 in which the scaling collapse of the energy gap distribution is obtained for $z=z'$ in accordance with Eq. (4). For $p > p_p$, the connected spin clusters are finite and isolated. Therefore the low-energy excitations are also localized.

VI. SUMMARY AND DISCUSSION

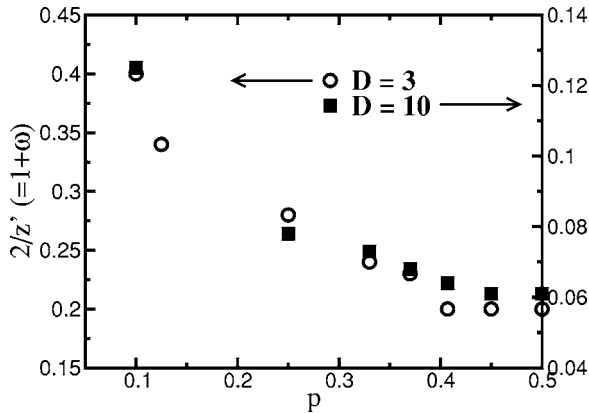In this paper we have studied the effect of strong bond disorder on the low-energy, long-distance properties of Heisenberg antiferromagnetic layers and bilayers with site and dimer dilution. In particular we are interested in the structure of the phase diagram and the form of the critical singularities as well as the properties of the Griffiths singularities.

In a single layer an order-disorder transition is found and the position of the transition point p^* appears to be independent of bond disorder strength D. This order-disorder transition appears to coincide with the percolation threshold $p=p_p$. However, on the basis of our numerical data we cannot strictly exclude the possibility that AF order is already destroyed for $p < p_p$—i.e., below the percolation threshold. Furthermore, the decay of the average spin-spin correlation function at the percolation threshold $p=p_p$ shows a power-law form with a strong-D-independent exponent $2\beta/\nu$ at $p=p_p$; this decay exponent is much smaller than the known exponent $2\beta/\nu=10/48$ for $D=0$. The dynamical exponent z

FIG. 13. The gap exponent ω in the diluted single-layer antiferromagnet ($g=0$) for different dilutions and bond disorder. Note that in the disordered phase, above the percolation threshold $p > p_p$, the gap exponent is practically independent of the dilution.
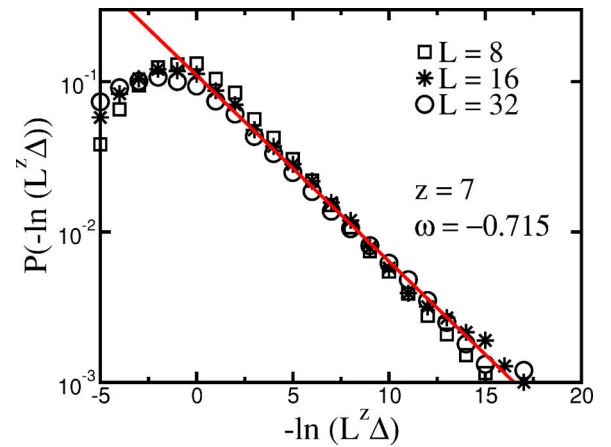

FIG. 14. (Color online) A finite-size scaling plot of the distribution of the logarithm of the energy gap for the double-layer antiferromagnet with a bilayer coupling $g=1$, bond randomness $D=8$, and dimer dilution concentration $p=0.125$. The dynamical exponent z and the slope $(-1-\omega)$ of small energy gaps agree well with the relation $z=2/(1+\omega)$, implying localized energy gaps.

of the diluted single layer is found to be a continuously increasing function of the disorder D. Here we note that in the limit of infinite D the fixed point becomes an infinite disorder fixed point with $z \to \infty$ so that the RG method is expected to be asymptotically exact with increasing D, as well supported by comparing with QMC results.

In the dimer-diluted bilayer with $g > 0$, weak disorder is found not to modify the static critical exponent β/ν as well as the dynamical exponent z, which are—within the error bars—the same as one measures at the fixed point B. On the other hand, for strong bond disorder the critical bilayer coupling is reduced to a very small value and both the static and dynamical exponents are different than for weak disorder. While the static exponent approaches a D-independent limiting value, the dynamical exponent shows a linear D dependence.

Considering the Griffiths singularities the low-energy fixed point of the RG is found to depend on the specific form of the disorder. For example, the nondiluted single layer ($g = p = 0$) transforms into an effective singlet and the diluted single layer ($g = 0$, $0 < p < p_p$) into a large spin, whereas the dimer-diluted bilayer also transforms into an effective singlet. In each case the disorder-induced dynamical exponent is found D dependent for sufficiently large D. For smaller values of D the true dynamical exponent is determined by quantum fluctuations, so that in this region disorder can influence only the corrections to scaling. The low-energy excitations are found to be nonlocalized for weak bond disorder as well as in the large-spin phase and become localized only for substantially large disorder.

[1] See, e.g., E. Fradkin, *Field Theories of Condensed Matter Systems* (Addison-Wesley, Palo Alto, CA, 1991).

[2] N. D. Mermin and H. Wagner, Phys. Rev. Lett. **17**, 1133 (1966).

[3] H. Neuberger and T. Ziman, Phys. Rev. B **39**, 2608 (1989); M. Gross, E. Sánchez-Velasco, and E. D. Siggia, *ibid.* **40**, 11328 (1989).

[4] S. Chakravarty, B. I. Halperin, and D. R. Nelson, Phys. Rev. B **39**, 2344 (1989).

[5] N. Read and S. Sachdev, Phys. Rev. Lett. **62**, 1694 (1989).

[6] R. R. P. Singh, M. P. Gelfand, and D. A. Huse, Phys. Rev. Lett. **61**, 2484 (1988).

[7] K. Hida, J. Phys. Soc. Jpn. **59**, 2230 (1990); **61**, 1013 (1992).

[8] A. J. Millis and H. Monien, Phys. Rev. Lett. **70**, 2810 (1993).

[9] A. W. Sandvik and D. J. Scalapino, Phys. Rev. Lett. **72**, 2777 (1994).

[10] D. C. Johnston, J. P. Stokes, D. P. Goshorn, and J. T. Lewandowski, Phys. Rev. B **36**, 4007 (1987); S.-W. Cheong, A. S. Cooper, L. W. Rupp, B. Batlogg, J. D. Thompson, and Z. Fisk, *ibid.* **44**, 9739 (1991); M. Corti, A. Rigamonti, F. Tabak, P. Carretta, F. Licci, and L. Raffo, *ibid.* **52**, 4226 (1995); O. P. Vajk, P. K. Mang, M. Greven, P. M. Gehring, and J. W. Lynn, Science **295**, 169 (2002).

[11] A. W. Sandvik, Phys. Rev. Lett. **86**, 3209 (2001); Phys. Rev. B **66**, 024418 (2002).

[12] A. W. Sandvik, Phys. Rev. Lett. **96**, 207201 (2006).

[13] A. W. Sandvik, Phys. Rev. Lett. **89**, 177201 (2002).

[14] O. P. Vajk and M. Greven, Phys. Rev. Lett. **89**, 177202 (2002).

[15] R. Sknepnek, T. Vojta, and M. Vojta, Phys. Rev. Lett. **93**, 097201 (2004).

[16] For a review of the strong-disorder RG method, see F. Iglói and C. Monthus, Phys. Rep. **412**, 277 (2005).

[17] S. K. Ma, C. Dasgupta, and C.-K. Hu, Phys. Rev. Lett. **43**, 1434 (1979); C. Dasgupta and S. K. Ma, Phys. Rev. B **22**, 1305 (1980).

[18] D. S. Fisher, Phys. Rev. B **51**, 6411 (1995).

[19] D. Fisher, Physica A **263**, 222 (1999); O. Motrunich, S.-C. Mau, D. A. Huse, and D. S. Fisher, Phys. Rev. B **61**, 1160 (2000).

[20] D. S. Fisher, Phys. Rev. B **50**, 3799 (1994).

[21] R. A. Hyman, K. Yang, R. N. Bhatt, and S. M. Girvin, Phys. Rev. Lett. **76**, 839 (1996).

[22] E. Westerberg, A. Furusaki, M. Sigrist, and P. A. Lee, Phys. Rev. B **55**, 12578 (1997).

[23] Y.-C. Lin, R. Mélin, H. Rieger, and F. Iglói, Phys. Rev. B **68**, 024424 (2003).

[24] J. D. Reger and A. P. Young, Phys. Rev. B **37**, 5978 (1988).

[25] L. Wang, K. S. D. Beach, and A. W. Sandvik, Phys. Rev. B **73**, 014431 (2006).

[26] C. Yasuda and A. Oguchi, J. Phys. Soc. Jpn. **66**, 2836 (1997); **68**, 2773 (1999); Y.-C. Chen and A. H. Castro Neto, Phys. Rev. B **61**, R3772 (2000).

[27] R. Mélin, Y.-C. Lin, P. Lajkó, H. Rieger, and F. Iglói, Phys. Rev. B **65**, 104415 (2002).

[28] T. Hikihara, A. Furusaki, and M. Sigrist, Phys. Rev. B **60**, 12116 (1999).

[29] O. F. Syljuåsen and A. W. Sandvik, Phys. Rev. E **66**, 046701 (2002).

[30] P. Peczak, A. M. Ferrenberg, and D. P. Landau, Phys. Rev. B **43**, 6087 (1991).

[31] D. Stauffer and A. Aharony, *Introduction to Percolation Theory* (Taylor & Francis, London, 1991).

[32] Anisotropic dilution can also destroy the AF long-range order in the percolation cluster. See R. Yu, T. Roscilde, and S. Haas, Phys. Rev. B **73**, 064406 (2006).

[33] N. Laflorencie *et al.* (unpublished).

[34] N. Laflorencie, S. Wessel, A. Läuchli, and H. Rieger, Phys. Rev. B **73**, 060403(R) (2006).

[35] R. Juhász, Y.-C. Lin, and F. Iglói, Phys. Rev. B **73**, 224206 (2006).

[36] J. Galambos, *The Asymptotic Theory of Extreme Order Statistics* (John Wiley and Sons, New York, 1978).

[37] E. Yusuf and K. Yang, Phys. Rev. B **65**, 224428 (2002).

[38] We have checked that in the temperature range presented here the results for the 32×32 lattice are size independent.

[39] W. Marshall, Proc. R. Soc. London, Ser. A **232**, 48 (1955).

[40] M. Sigrist and A. Furusaki, J. Phys. Soc. Jpn. **65**, 2385 (1996).

[41] E. Yusuf and K. Yang, Phys. Rev. B **67**, 144409 (2003).